Vol 461|1 October 2009|doi:10.1038/nature08455

LETTERS

Discovery of Atg5/Atg7-independent alternative macroautophagy

Yuya Nishida[1,2]*, Satoko Arakawa[1]*, Kenji Fujitani[1], Hirofumi Yamaguchi[1], Takeshi Mizuta[1], Toku Kanaseki[1], Masaaki Komatsu[4], Kinya Otsu[3], Yoshihide Tsujimoto[2] & Shigeomi Shimizu[1]

Macroautophagy is a process that leads to the bulk degradation of subcellular constituents by producing autophagosomes/autolysosomes[1–3]. It is believed that *Atg5* (ref. 4) and *Atg7* (ref. 5) are essential genes for mammalian macroautophagy. Here we show, however, that mouse cells lacking Atg5 or Atg7 can still form autophagosomes/autolysosomes and perform autophagy-mediated protein degradation when subjected to certain stressors. Although lipidation of the microtubule-associated protein light chain 3 (LC3, also known as Map1lc3a) to form LC3-II is generally considered to be a good indicator of macroautophagy[6], it did not occur during the Atg5/Atg7-independent alternative process of macroautophagy. We also found that this alternative process of macroautophagy was regulated by several autophagic proteins, including Unc-51-like kinase 1 (Ulk1) and beclin 1. Unlike conventional macroautophagy, autophagosomes seemed to be generated in a Rab9-dependent manner by the fusion of isolation membranes with vesicles derived from the *trans*-Golgi and late endosomes. *In vivo*, Atg5-independent alternative macroautophagy was detected in several embryonic tissues. It also had a function in clearing mitochondria during erythroid maturation. These results indicate that mammalian macroautophagy can occur through at least two different pathways: an Atg5/Atg7-dependent conventional pathway and an Atg5/Atg7-independent alternative pathway.

The biological functions of macroautophagy have been examined by generating mice lacking several *Atg* genes, including *Atg5* (ref. 4), beclin 1 (*Becn1*)[7,8] and *Atg7* (ref. 5), considered essential for macroautophagy; constitutive and starvation-induced autophagy is impaired in such mice. However, because $Atg5^{-/-}$ or $Atg7^{-/-}$ mice remain healthy until the perinatal period[4,5], an alternative mechanism of bulk protein degradation may compensate for the lack of Atg5/Atg7-dependent macroautophagy.

To investigate possible alternative protein degradation mechanisms in $Atg5^{-/-}$ mice, we obtained embryonic fibroblasts from *Atg5* knockout mice ($Atg5^{-/-}$ MEFs) and their control littermates (wild-type (WT) MEFs) (Supplementary Fig. 2a). Treatment with rapamycin induced macroautophagy in WT MEFs but not in $Atg5^{-/-}$ MEFs (Supplementary Fig. 2b), as reported previously[9]. We investigated autophagy induced by cytotoxic stressors (such as etoposide). After exposure to etoposide, each cell detached and underwent apoptosis in the same proportion (Supplementary Fig. 3). To exclude apoptotic consequences, only attached MEFs were examined. Etoposide resulted in the formation of numerous autophagic vacuoles in WT MEFs (Supplementary Fig. 2c), and an equivalent size and number of autophagic vacuoles also appeared in $Atg5^{-/-}$ MEFs (Fig. 1a (electron microscopy, EM), b and Supplementary Fig. 2c). The autophagic area in each cell increased equivalently over time during exposure to etoposide in WT and $Atg5^{-/-}$ MEFs (Fig. 1c). Typical autophagic structures, including double-membrane structures, autophagosomes, amphisomes[10,11] and autolysosomes, were observed in etoposide-treated $Atg5^{-/-}$ MEFs (Fig. 1d and Supplementary Fig. 4a). The presence of multilamellar bodies in autolysosomes indicated autophagic degradation of subcellular constituents (Fig. 1d). These autolysosomal structures were merged with the immunofluorescence dots of Lamp2, a lysosomal protein (Fig. 1a and Supplementary Fig. 5). There were numerous double-membrane structures and few autolysosomes in $Atg5^{-/-}$ MEFs after treatment with etoposide for 12 h; the situation was reversed at 18 h (Supplementary Fig. 4b), indicating that the autophagic process progressed over time after exposure to etoposide. Similar structures were observed when cells were examined by electron microscopy after quick freezing and freeze-substitution, a technique that achieves superior preservation of cellular architecture (Fig. 1e and Supplementary Fig. 4a). Similar results were observed when apoptosis was inhibited by the pan-caspase inhibitor zVAD-fmk (see later). Furthermore, similar macroautophagy was observed in etoposide-treated $Atg5^{-/-}$ MEFs from a different $Atg5^{-/-}$ mouse (Supplementary Fig. 6a, b) and in staurosporine-treated $Atg5^{-/-}$ MEFs and $Atg5^{-/-}$ thymocytes (Supplementary Fig. 6c, d). This suggests that cells possess the Atg5-independent macroautophagy system, designated 'alternative macroautophagy'.

To confirm the induction of alternative macroautophagy in etoposide-treated $Atg5^{-/-}$ MEFs, we examined the effect of bafilomycin A1, which prevents the fusion of autophagosomes with lysosomes[12]. Exposure to bafilomycin A1 was expected to increase and decrease the number of autophagosomes and autolysosomes, respectively. We obtained the expected results in WT MEFs and $Atg5^{-/-}$ MEFs, supporting the notion of Atg5-independent induction of macroautophagy (Fig. 1f and Supplementary Fig. 7a). Moreover, 3-methyladenine, a phosphatidylinositol-3-OH kinase (PI(3)K) inhibitor that blocks Atg5-dependent autophagosome formation[13], significantly suppressed autophagosome formation in etoposide-treated $Atg5^{-/-}$ MEFs (Fig. 1g and Supplementary Fig. 7b), suggesting the involvement of PI(3)K in Atg5-independent macroautophagy.

We next assessed whether and to what extent protein degradation occurs in etoposide-treated $Atg5^{-/-}$ MEFs. Etoposide induced protein degradation and had a similar effect on WT and $Atg5^{-/-}$ MEFs (Fig. 1h), which is consistent with the morphological analysis (Fig. 1c). Suppression of protein degradation by bafilomycin A1 and a lysosomal protease inhibitor cocktail suggested the involvement of lysosomal proteases (Fig. 1i). Although lysosomal proteases are also involved in macroautophagy-independent proteolysis, including chaperone-mediated autophagy[14], alternative macroautophagy may possibly have functioned in etoposide-induced proteolysis, because protein degradation was suppressed by 3-methyladenine (Fig. 1i),

[1]Department of Pathological Cell Biology, Medical Research Institute, Tokyo Medical and Dental University, 1-5-45 Yushima, Bunkyo-ku, Tokyo 113-8510, Japan. [2]Department of Medical Genetics, [3]Department of Cardiovascular Medicine, Osaka University Medical School, 2-2 Yamadaoka, Suita, Osaka 565-0871, Japan. [4]Laboratory of Frontier Science, Tokyo Metropolitan Institute of Medical Science, Bunkyo-ku, Tokyo 113-8613, Japan.
*These authors contributed equally to this work.

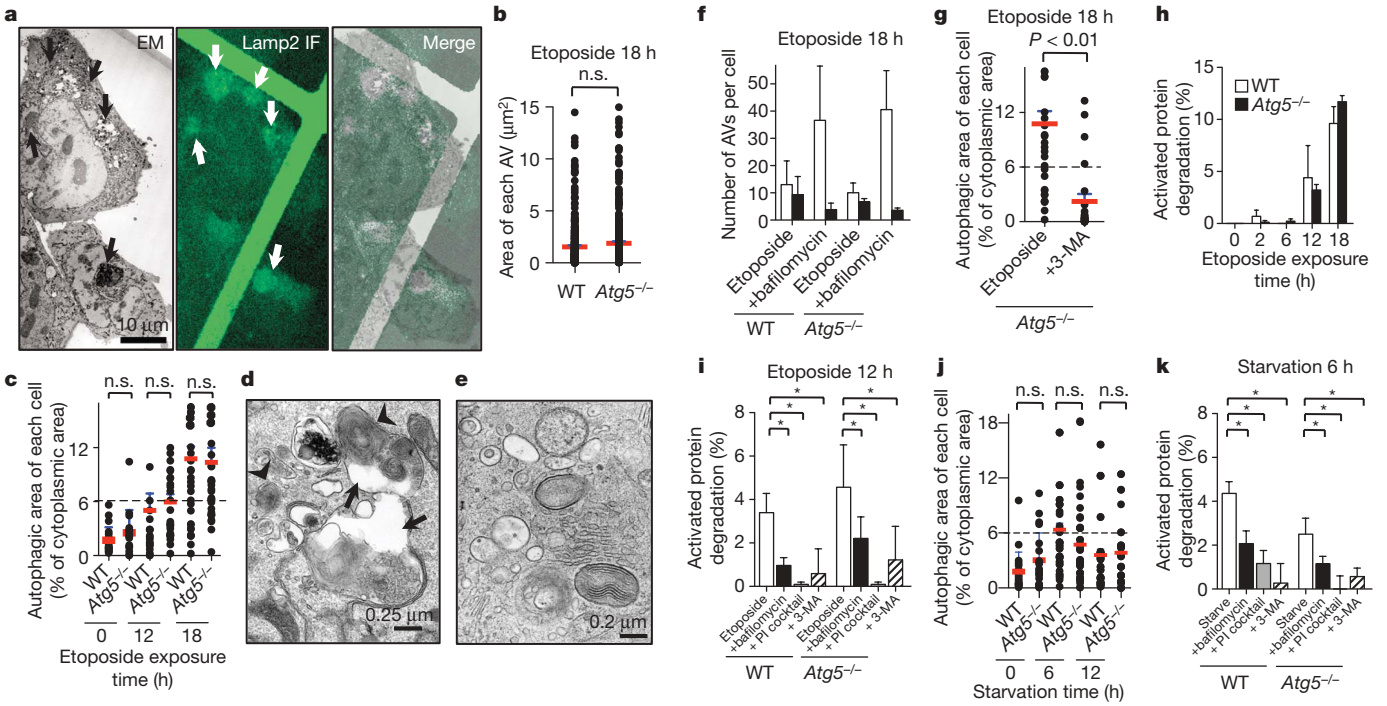

Figure 1 | Induction of macroautophagy in *Atg5*$^{-/-}$ MEFs by etoposide and starvation. **a**, Etoposide-treated *Atg5*$^{-/-}$ MEFs were assessed by EM (left) and by Lamp2 immunofluorescence (IF; middle). Right: reverse Lamp2 immunofluorescence image merged with the electron microscopy image. Arrows indicate Lamp2-positive autolysosomes. Magnified photos are provided in Supplementary Fig. 5. **b**, The size of each autophagic vacuole (AV) ($n = 30$ cells) in MEFs treated with etoposide. The total number of AVs in 30 cells was 483 in WT cells and 494 in *Atg5*$^{-/-}$ cells. **c**, Percentage autophagic area ($n \geq 20$ cells) in MEFs treated with etoposide. **d**, **e**, Representative macroautophagy in etoposide-treated *Atg5*$^{-/-}$ MEFs. Conventional (**d**) and quick freezing and freeze-substitution (**e**) techniques were used. The autolysosomes (arrows) contain multilamellar bodies (arrowheads). **f**, The number of autophagosomes (white columns) and autolysosomes (black columns) in MEFs ($n = 10$ cells) treated with etoposide. **g**, Reduction of percentage autophagic area by 3-methyladenine (3-MA; $n = 22$ cells). **h**, Time-course analysis of long-lived protein degradation ($n = 4$). **i**, Inhibition of long-lived protein degradation by bafilomycin A1, protease inhibitor (PI) cocktail and 3-MA (*$P < 0.05$; $n = 4$). **j**, **k**, Similar experiments to those in **c** and **i** were performed by starvation. Red and blue lines in **b**, **c**, **g** and **j** indicate means and s.e.m., respectively. The dashed line in **c**, **g** and **j** indicates the autophagic cell border (6%). Black error bars indicate s.d.

which blocked macroautophagy (Fig. 1g) but not chaperone-mediated autophagy[14]. zVAD-fmk was used in these experiments to avoid the influence of apoptosis-related proteolysis; its addition did not influence etoposide-induced macroautophagy (Supplementary Fig. 8).

We investigated starvation-induced Atg5-independent macroautophagy. Although a lack of autophagosomes in *Atg5*$^{-/-}$ cells has been reported for embryonic stem cells[15], we found mature autophagic vacuoles in starved *Atg5*$^{-/-}$ MEFs (Supplementary Fig. 9a). The extent of this macroautophagy was slightly less than that in starved WT MEFs (Fig. 1j, k and Supplementary Fig. 9b, c). Protein degradation in starved *Atg5*$^{-/-}$ MEFs was inhibited by bafilomycin A1, protease inhibitor cocktail and 3-methyladenine (Fig. 1k), indicating that starvation-induced proteolysis was also mediated by alternative macroautophagy in *Atg5*$^{-/-}$ MEFs. Mammalian macroautophagy can therefore occur through two pathways—Atg5-dependent conventional and Atg5-independent alternative pathways—possibly activated by different stimuli.

We examined whether autophagic modification of LC3 occurs during Atg5-independent alternative macroautophagy. LC3-II, a lipid conjugate form, and a punctate fluorescence pattern of green fluorescent protein (GFP)-tagged LC3 were observed in WT MEFs but not in *Atg5*$^{-/-}$ MEFs during treatment with etoposide (Fig. 2a–c), suggesting an absence of LC3 modification in alternative macroautophagy. This was confirmed by observing GFP–LC3 fluorescence followed by electron microscopy analysis in the same *Atg5*$^{-/-}$ MEFs. Autophagic vacuoles were generated in etoposide-treated *Atg5*$^{-/-}$ MEFs (Fig. 2d, EM); GFP–LC3 was distributed homogeneously throughout these cells (Fig. 2d, GFP–LC3). Mammalian cells have two other yeast Atg8 homologues, Gabarap and Gabarapl2 (ref. 16). Examination with yellow fluorescent protein (YFP)-tagged Gabarap and YFP–Gabarapl2 yielded results similar to those for GFP–LC3 (Supplementary Fig. 10). WT and *Atg5*$^{-/-}$ MEFs showed similar macroautophagy levels after exposure to etoposide (Fig. 1c), even though both macroautophagy types were activated in WT MEFs (Supplementary Fig. 11) and only the alternative form was activated in *Atg5*$^{-/-}$ MEFs; however, this may have resulted from the mutual regulation between conventional and alternative macroautophagy.

Immunostaining was performed for Lamp2 to assess the extent of alternative macroautophagy in etoposide-treated *Atg5*$^{-/-}$ MEFs, because the fluorescence pattern changed from diffuse to punctate during autolysosome generation (Fig. 2e). The following evidence supports the validity of this assay: first, the Lamp2 fluorescent dots coincided with autolysosomes (Fig. 1a); second, the number of *Atg5*$^{-/-}$ MEFs with fluorescent dots matched that of autophagic cells assessed by electron microscopy (Supplementary Fig. 12a); and third, bafilomycin A1 decreased the number of cells with dots (Supplementary Fig. 12b). We searched for molecules involved in alternative macroautophagy by using the Lamp2 immunostaining assay. Because many DNA damage-induced events are under transcriptional regulation, we compared the gene expression profiles of healthy and etoposide-treated *Atg5*$^{-/-}$ MEFs. The autophagic molecule Ulk1 (ref. 17) was upregulated in etoposide-treated *Atg5*$^{-/-}$ MEFs (Fig. 2f) and confirmed by quantitative PCR with reverse transcription (qRT–PCR) (Fig. 2g) and western blotting (Fig. 2h). Furthermore, silencing both Ulk1 and Fip200 (also known as Rb1cc1)—a component of the Ulk1 kinase complex[18]—decreased the number of autophagic cells (Fig. 2i, j and Supplementary Fig. 13), indicating that the Ulk1 complex is important in alternative macroautophagy.

Because Ulk1 is involved in alternative macroautophagy, some conventional autophagy-related molecules might function in the alternative process. Conventional macroautophagy machinery includes the Ulk1 complex[18], the PI(3)K complex, the Atg9 systems

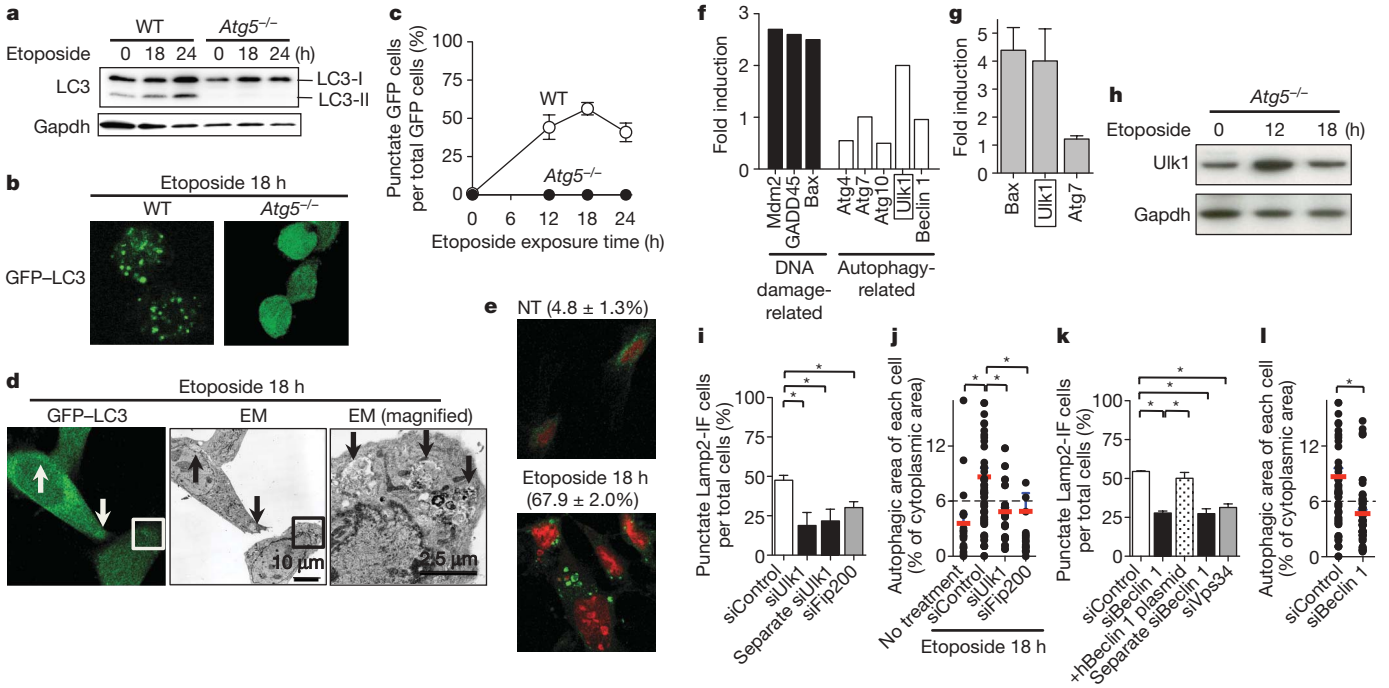

Figure 2 | Involvement of the Ulk1 and PI(3)K complexes in etoposide-induced alternative macroautophagy. **a**, The production of LC3-II. Gapdh was used as a loading control. **b**, **c**, Punctate GFP–LC3 fluorescence in WT MEFs but not in *Atg5*$^{-/-}$ MEFs. **b**, Representative photographs. **c**, Graphical presentation of the percentages of WT MEFs and *Atg5*$^{-/-}$ MEFs with punctate GFP–LC3 fluorescence. **d**, The same GFP–LC3-transfected *Atg5*$^{-/-}$ MEFs were assessed by IF and by EM. The magnified photo is the area indicated by the squares. Arrows indicate AVs. **e**, *Atg5*$^{-/-}$ MEFs were incubated without (NT) or with etoposide and immunostained with an anti-Lamp2 antibody (green). Nuclei were counterstained (red). The percentages of cells with punctate Lamp2 immunostaining are shown (means ± s.d., $n = 4$). **f**, Microarray analysis of the *Atg5*$^{-/-}$ MEFs during treatment with etoposide. **g**, **h**, Induction of Ulk1 in the etoposide-treated *Atg5*$^{-/-}$ MEFs was assessed by qPCR (**g**) and by immunoblotting (**h**). **i**–**l**, *Atg5*$^{-/-}$ MEFs were transfected with the siRNAs related to the Ulk1 complex (**i**, **j**) and the PI(3)K complex (**k**, **l**) and a beclin 1 plasmid (**k**) for 24 h and treated with etoposide for 18 h. Induction of macroautophagy was assessed by Lamp2 IF (**i**, **k**) and by EM (**j**, **l**). In **i** and **k**, $^*P < 0.05$ ($n = 4$); in **j** and **l**, $^*P < 0.01$ ($n = 35$ cells each). hBeclin 1, human beclin 1. Red and blue lines in **j** and **l** indicate means and s.e.m., respectively. The dashed line in **j** and **l** indicates the autophagic cell border. Black error bars indicate s.d. ($n = 4$). Original magnification (**b**, **e**), × 200.

and two Atg7-mediated ubiquitin-like protein systems (Atg8 and Atg12 is conjugated with phosphatidylethanolamine and Atg5, respectively, and Atg16 interacts with Atg5)[2]. When *Atg7*$^{-/-}$ MEFs were treated with etoposide, macroautophagy was induced without generating LC3-II (Supplementary Fig. 14). Moreover, silencing of Atg7, Atg12 or Atg16 did not suppress alternative macroautophagy in *Atg5*$^{-/-}$ MEFs (Supplementary Fig. 15). Together with the data on Atg5 and Atg8 homologues, these experiments indicated that the ubiquitin-like protein systems are not required for alternative macroautophagy. In addition, silencing of Atg9 did not show any influence (Supplementary Fig. 15). In contrast, silencing of beclin 1 decreased the number of autophagic cells (Fig. 2k, l and Supplementary Fig. 16). The involvement of beclin 1 was further confirmed by the restoration of macroautophagy after overexpression of human beclin 1 in beclin 1-silenced *Atg5*$^{-/-}$ MEFs (Fig. 2k). Silencing of Vps34, another component of the PI(3)K complex, decreased the number of autophagic cells (Fig. 2k and Supplementary Fig. 16), indicating that the complex is involved in etoposide-induced alternative macroautophagy; this is consistent with the data for 3-methyladenine (Fig. 1g, i). Ulk1, Fip200, beclin 1 and Vps34 (but not Atg7, Atg12, Atg16 or Atg9) were involved in alternative macroautophagy induced by starvation (Supplementary Fig. 17a) and staurosporine (Supplementary Fig. 17b).

The following observations were also noted: first, almost all autophagic vacuoles were localized near the Golgi apparatus (Fig. 3a, b); second, some isolation membranes extended from the Golgi membranes (Fig. 3a, inset); third, closure of some isolation membranes occurred by fusion with vesicles with thicker membranes[19], presumably derived from the *trans*-Golgi (*trans*-Golgi cisternae and *trans*-Golgi network) (Fig. 3c, d); and fourth, inhibition of Golgi-derived membrane by brefeldin A resulted in the inhibition of alternative but not conventional macroautophagy (Supplementary Fig. 18). We therefore examined the involvement of the *trans*-Golgi or endosomes in the extension and closure of isolation membranes. First, we introduced genes encoding GFP-tagged organelle marker proteins into *Atg5*$^{-/-}$ MEFs and analysed the co-localization with Lamp2-positive vacuoles. Etoposide induced the redistribution of a fraction of mannose 6-phosphate receptors (a marker for the *trans*-Golgi and late endosomes[20]); it was co-localized with Lamp2-positive autolysosomes (Fig. 3e and Supplementary Fig. 19a). Similar results were observed with TGN38 (a marker for the *trans*-Golgi network[20]) (Supplementary Fig. 19b) and syntaxin 7 (a marker for late endosomes) (Fig. 3e and Supplementary Fig. 19a) but not calnexin (a marker for the endoplasmic reticulum) (Supplementary Fig. 19c), confirming the involvement of the *trans*-Golgi or late endosomes in alternative macroautophagy. Because Rab9 is involved in trafficking from late endosomes to the *trans*-Golgi[20], we suspected its role in alternative macroautophagy. As expected, GFP–Rab9 was co-localized with Lamp2-positive autolysosomes in etoposide-treated *Atg5*$^{-/-}$ MEFs (Fig. 3f and Supplementary Fig. 20a). This co-localization was slightly increased with GFP–Rab9(Q66L), a GTP-preferring active Rab9 form[20], and decreased with GFP–Rab9(S21N), a GDP-preferring dominant-negative Rab9 form[20] (Supplementary Fig. 20b). Furthermore, Rab9 silencing (Supplementary Fig. 20c) decreased etoposide-induced alternative macroautophagy (Fig. 3g, h and Supplementary Fig. 20d, e), indicating that Rab9 is involved in Atg5-independent macroautophagy. Rab9 silencing decreased the number of autophagic vacuoles but induced the accumulation of isolation membranes (Fig. 3i). Because many isolation membranes were normally generated from the early exposure to etoposide (Fig. 3i), the effect of Rab9 silencing was not due merely to a slow progression of macroautophagy but also to inhibition of autophagosome maturation. This accumulation of

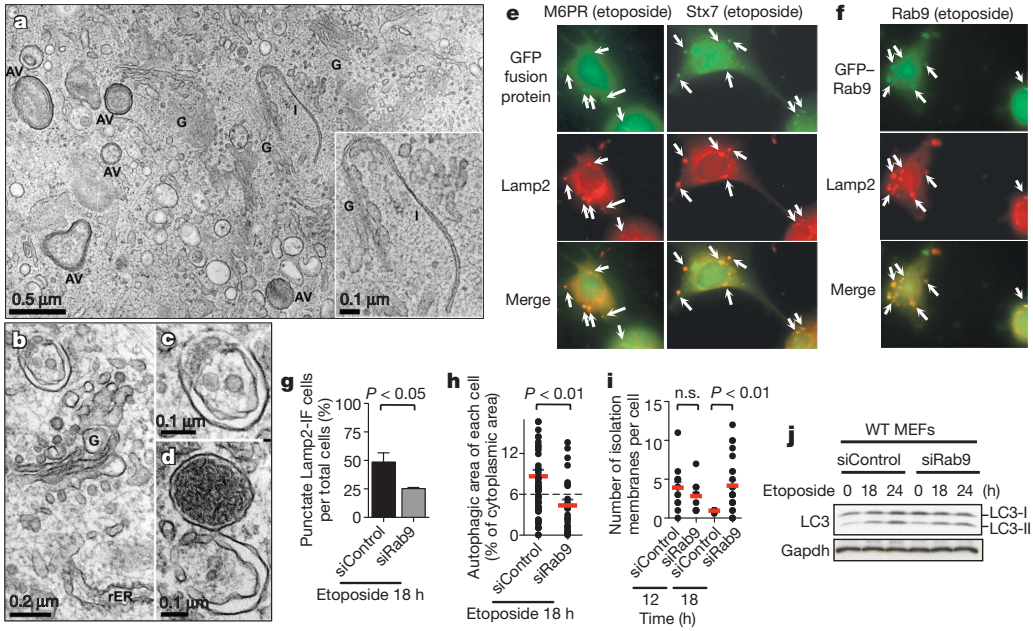

Figure 3 | Involvement of Rab9 in alternative autophagosome generation. **a–d**, Electron micrographs of etoposide-treated $Atg5^{-/-}$ MEFs. **a**, AVs were observed near the Golgi apparatus (G). Inset, the isolation membrane (I) was extended from the Golgi stack. **b**, Developing autophagosome. rER, rough endoplasmic reticulum. **c**, **d**, Isolation membrane fusing with vesicles containing thick membrane (**d**) and a complete autophagosome (**c**) is generated. **e**, **f**, Co-localization of Lamp2 with GFP–M6PR, GFP–Stx7 or GFP–Rab9 in etoposide-treated $Atg5^{-/-}$ MEFs. Arrows indicate co-localized dots. Original magnification, × 200. **g–i**, $Atg5^{-/-}$ MEFs were transfected with the indicated siRNAs for 24 h and treated with etoposide. Induction of macroautophagy was assessed by Lamp2 IF (**g**) and by EM (**h**), and the number of isolation membranes was calculated (**i**). In **g**, error bars indicate s.d. ($n = 4$). In **h** and **i**, red and blue lines indicate means and s.e.m., respectively; $n = 35$ cells each. **j**, No effect of silencing of Rab9 (siRab9) on the production of LC3-II in etoposide-treated WT MEFs.

isolation membranes was not observed with Ulk1 silencing (Supplementary Fig. 13d) or beclin 1 silencing (Supplementary Fig. 16d). Rab9 silencing had no influence on conventional macroautophagy (Fig. 3j), indicating that Rab9 is required for alternative but not conventional macroautophagy.

Finally, we examined alternative macroautophagy in $Atg5^{-/-}$ embryos to understand its physiological relevance. In $Atg5^{-/-}$ fetal brains (Fig. 4a), livers (Fig. 4b–d) and hearts (Fig. 4e), we detected autophagic vacuoles at the same level as in WT fetal tissues (data not shown). We then investigated alternative macroautophagy during erythrocyte maturation. Erythrocytes undergo organelle clearance during terminal differentiation, and macroautophagy may function in this process[21,22]. In fact, ultrastructural analysis of the WT fetal liver (embryonic day (E)14.5), where haematopoiesis occurs, showed that autophagic vacuoles in reticulocytes engulfed and digested mitochondria (Fig. 4f). We observed a few more autophagic vacuoles in $Atg5^{-/-}$ reticulocytes (Fig. 4g–i). Examination of the circulating erythrocytes showed that although the number of autophagic vacuoles was decreased, a few mitochondria were still engulfed and digested in the vacuoles in both mice groups (Fig. 4k–n). Moreover, the number of persisting mitochondria in $Atg5^{-/-}$ reticulocytes and erythrocytes was the same as in WT cells of each type (Fig. 4j, o).

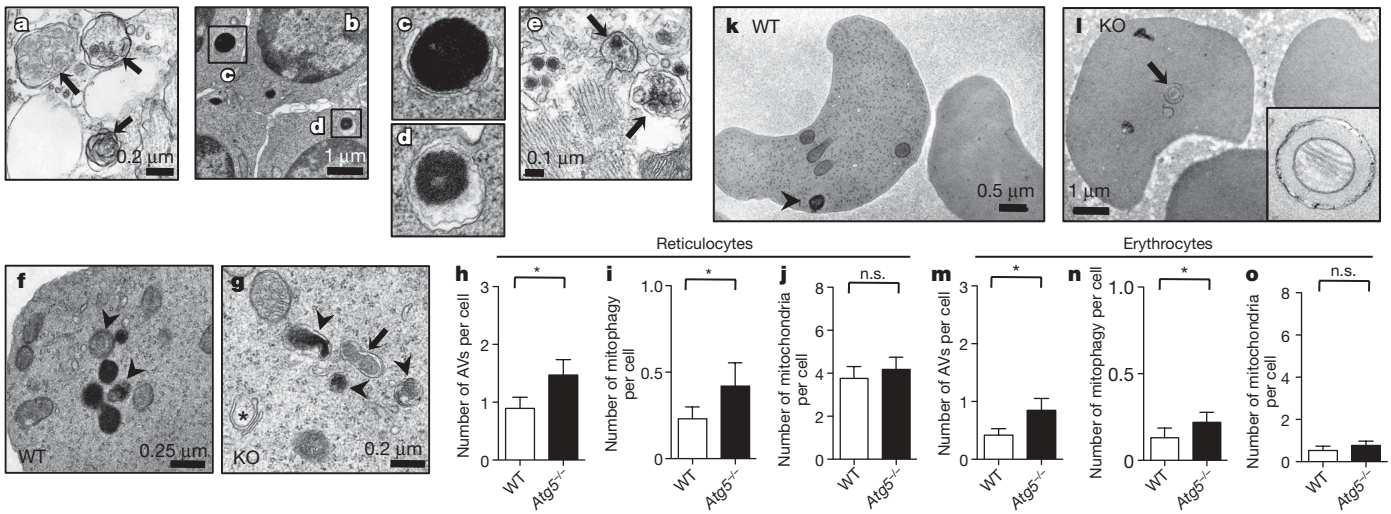

Figure 4 | Physiological roles of alternative macroautophagy. **a–e**, Typical autophagic structures in the tissues of an $Atg5^{-/-}$ embryo (E14.5): **a**, midbrain; **b–d**, liver; **c**, **d**, developing autophagosomes; **e**, heart. Arrows indicate the autophagic vacuoles. **f**, **g**, **k**, **l**, Electron micrographs of wild-type (WT) and $Atg5^{-/-}$ (KO) reticulocytes (**f**, **g**) and erythrocytes (**k**, **l**). An isolation membrane (asterisk), autophagosomes (arrows) and autolysosomes (arrowheads) are shown. Inset, engulfed mitochondria. **h–j**, **m–o**, The numbers of autophagic vacuoles (**h**, **m**) and autophagic vacuoles containing mitochondria (**i**, **n**) and persisting mitochondria (**j**, **o**) in reticulocytes (**h–j**) and erythrocytes (**m–o**). Error bars indicate s.d. (*$P < 0.05$; $n = 55$ cells).

This was confirmed when residual mitochondria were examined by MitoTracker Green in Ter119$^+$ erythroid cells (Supplementary Fig. 21a), which is consistent with previous findings[23]. Similar results were observed when different mice were analysed (Supplementary Fig. 21b). Furthermore, Ter119$^+$ CD71$^+$ and Ter119$^+$ CD71$^-$ erythroid cell populations were similar in WT and *Atg5*$^{-/-}$ mice, indicating that terminal differentiation proceeded equally (Supplementary Fig. 21c). Mitochondrial clearance from erythroid cells may be due to Atg5-independent alternative macroautophagy. This is consistent with observations that a lack of Ulk1 and the addition of 3-methyladenine results in disturbance in autophagic clearance of mitochondria[22,24]. Taken together, these results show that Ulk1-mediated alternative macroautophagy may function in the terminal differentiation of erythrocytes.

Our findings indicate that macroautophagy is more complex than previously realized. Conventional macroautophagy is crucial for basal and starvation-induced autophagy *in vitro*[4,5], and is required for neuronal protein aggregate clearance[25,26] and overcoming early neonatal starvation *in vivo*[4,5]. In contrast, we showed that alternative macroautophagy can be triggered by cellular stress *in vitro* and that it functions in the autophagic elimination of organelles during erythrocyte differentiation *in vivo*. Although both processes lead to the bulk degradation of cellular proteins, they may be activated by different stimuli in different cell types and may have different physiological functions. To understand macroautophagy better, it is important to classify autophagy-related molecules according to the type of macroautophagy in which they are involved.

METHODS SUMMARY

DNA transfection. MEFs were transfected with plasmid DNAs or short interfering RNAs (siRNAs) with the Amaxa electroporation system[27]. In some experiments, plasmids were introduced into MEFs by retroviral infections by using Plat-E cells.

Induction of autophagy. MEFs were treated with 10 μM etoposide for 18 h or starved for 6 h, unless otherwise indicated.

Electron microscopy. Cells and tissues were fixed by a conventional method or by a quick-freeze substitution method. Fixed samples were embedded in Epon 812, and thin sections were then cut and stained with uranyl acetate and lead citrate for observation under a Jeol-1010 electron microscope (Jeol) at 80 kV. The area of every autophagic vacuole and the total cytoplasmic area were calculated on the photographs by using a planimeter. For each cell, the autophagic area was calculated by expressing the total area of autophagic vacuoles as a percentage of the cytoplasmic area. In experiments combining fluorescence microscopy and electron microscopy, cells were cultured on coverslips with grids and fixed with paraformaldehyde and glutaraldehyde. In the Lamp2 experiment, cells were then immunostained with anti-Lamp2 monoclonal antibody. Subsequently, some sections were viewed under a confocal fluorescence microscope; the cells were fixed with OsO_4 and examined by electron microscopy. In the GFP–LC3 experiment, after GFP–LC3 fluorescence had been viewed, the same cells were fixed with OsO_4 and examined by electron microscopy.

Long-lived protein degradation assay. MEFs were starved or treated with etoposide with zVAD-fmk (100 μM), and the degradation of long-lived proteins was measured by a standard method[28]. The extent of protein degradation was calculated as the percentage of protein degradation in stress-induced cells minus the percentage of protein degradation in healthy cells.

Immunofluorescence analysis. Cells were fixed in 4% formaldehyde, permeabilized in 0.1% Triton X-100 and stained with anti-Lamp2 monoclonal antibody, followed by a FITC-conjugated secondary antibody.

Full Methods and any associated references are available in the online version of the paper at www.nature.com/nature.

Received 5 May; accepted 24 August 2009.

1. Mizushima, N., Levine, B., Cuervo, A. M. & Klionsky, D. J. Autophagy fights disease through cellular self-digestion. *Nature* **451,** 1069–1075 (2008).
2. Xie, Z. & Klionsky, D. J. Autophagosome formation: core machinery and adaptations. *Nature Cell Biol.* **9,** 1102–1109 (2007).
3. Mizushima, N., Ohsumi, Y. & Yoshimori, T. Autophagosome formation in mammalian cells. *Cell Struct. Funct.* **27,** 421–429 (2002).
4. Kuma, A. *et al.* The role of autophagy during the early neonatal starvation period. *Nature* **432,** 1032–1036 (2004).
5. Komatsu, M. *et al.* Impairment of starvation-induced and constitutive autophagy in Atg7-deficient mice. *J. Cell Biol.* **169,** 425–434 (2005).
6. Kabeya, Y. *et al.* LC3, a mammalian homologue of yeast Apg8p, is localized in autophagosome membranes after processing. *EMBO J.* **19,** 5720–5728 (2000).
7. Yue, Z., Jin, S., Yang, C., Levine, A. J. & Heintz, N. Beclin 1, an autophagy gene essential for early embryonic development, is a haploinsufficient tumor suppressor. *Proc. Natl Acad. Sci. USA* **100,** 15077–15082 (2003).
8. Qu, X. *et al.* Promotion of tumorigenesis by heterozygous disruption of the beclin 1 autophagy gene. *J. Clin. Invest.* **112,** 1809–1820 (2003).
9. Rosenbluth, J. M. & Pietenpol, J. A. mTOR regulates autophagy-associated genes downstream of p73. *Autophagy* **5,** 114–116 (2009).
10. Liou, W., Geuze, H. J., Geelen, M. J. H. & Slot, J. W. The autophagic and endocytic pathways converge at the nascent autophagic vacuoles. *J. Cell Biol.* **136,** 61–70 (1997).
11. Razi, M., Chan, E. Y. W. & Tooze, S. A. Early endosomes and endosomal coatomer are required for autophagy. *J. Cell Biol.* **185,** 305–321 (2009).
12. Yoshimori, T., Yamamoto, A., Moriyama, Y., Futai, M. & Tashiro, Y. Bafilomycin A1, a specific inhibitor of vacuolar-type H^+-ATPase, inhibits acidification and protein degradation in lysosomes of cultured cells. *J. Biol. Chem.* **266,** 17707–17712 (1991).
13. Bursch, W. The autophagosomal–lysosomal compartment in programmed cell death. *Cell Death Differ.* **8,** 569–581 (2001).
14. Cuervo, A. M. Autophagy: many paths to the same end. *Mol. Cell. Biochem.* **263,** 55–72 (2004).
15. Mizushima, N. *et al.* Dissection of autophagosome formation using Apg5-deficient mouse embryonic stem cells. *J. Cell Biol.* **152,** 657–668 (2001).
16. Kabeya, Y. *et al.* LC3, GABARAP and GATE16 localize to autophagosomal membrane depending on form-II formation. *J. Cell Sci.* **117,** 2805–2812 (2004).
17. Young, A. R. *et al.* Starvation and ULK1-dependent cycling of mammalian Atg9 between the TGN and endosomes. *J. Cell Sci.* **119,** 3888–3900 (2006).
18. Hara, T. *et al.* FIP200, a ULK-interacting protein, is required for autophagosome formation in mammalian cells. *J. Cell Biol.* **181,** 497–510 (2008).
19. Gagnon, E. Endoplasmic reticulum-mediated phagocytosis is a mechanism of entry into macrophages. *Cell* **110,** 119–131 (2002).
20. Riederer, M. A., Soldati, T., Shapiro, A. D., Lin, J. & Pfeffer, S. R. Lysosome biogenesis requires Rab9 function and receptor recycling from endosomes to the *trans*-Golgi network. *J. Cell Biol.* **125,** 573–582 (1994).
21. Fader, C. M. & Colombo, M. I. Multivesicular bodies and autophagy in erythrocyte maturation. *Autophagy* **2,** 122–125 (2006).
22. Sandoval, H. *et al.* Essential role for Nix in autophagic maturation of erythroid cells. *Nature* **454,** 232–235 (2008).
23. Matsui, M., Yamamoto, A., Kuma, A., Ohsumi, Y. & Mizushima, N. Organelle degradation during the lens and erythroid differentiation is independent of autophagy. *Biochem. Biophys. Res. Commun.* **339,** 485–489 (2006).
24. Kundu, M. *et al.* Ulk1 plays a critical role in the autophagic clearance of mitochondria and ribosomes during reticulocyte maturation. *Blood* **112,** 1493–1502 (2008).
25. Hara, T. *et al.* Suppression of basal autophagy in neural cells causes neurodegenerative disease in mice. *Nature* **441,** 885–889 (2006).
26. Komatsu, M. *et al.* Loss of autophagy in the central nervous system causes neurodegeneration in mice. *Nature* **441,** 880–884 (2006).
27. Shimizu, S. *et al.* Role of Bcl-2 family proteins in a non-apoptotic programmed cell death dependent on autophagy genes. *Nature Cell Biol.* **6,** 1221–1228 (2004).
28. Ogier-Denis, E., Houri, J. J., Bauvy, C. & Codogno, P. Guanine nucleotide exchange on heterotrimeric Gi3 protein controls autophagic sequestration in HT-29 cells. *J. Biol. Chem.* **271,** 28593–28600 (1996).

Supplementary Information is linked to the online version of the paper at www.nature.com/nature.

Acknowledgements We thank M. Narita and A. R. J. Young for critical reading of the manuscript; N. Mizushima for providing *Atg5*$^{+/-}$ mice and the expression plasmid of GFP–LC3; T. Yoshimori for the human beclin 1 expression plasmid; and T. Kitamura for providing Plat-E cells. This study was supported in part by the Program for Promotion of Fundamental Studies in Health Sciences of the National Institute of Biomedical Innovation (NIBIO), a grant for Creative Scientific Research, a grant for the 21st Century COE Program from the Japanese Ministry of Education, Science, Sports and Culture, a grant for Comprehensive Research on Aging and Health from the Japanese Ministry of Health, Labor and Welfare, and a grant for Solution-Oriented Research for Science and Technology (SORST) from the Japan Science and Technology Corporation. This study was also supported by grants from the Uehara Memorial Foundation, the Sagawa Foundation for Promotion of Cancer Research, the YASUDA Medical Foundation, the Astellas foundation for research on metabolic disorders, and the Foundation for Promotion of Cancer Research.

Author Contributions Y.N. performed the biochemical analyses. S.A. and T.K. performed the electron microscopy analyses. K.F. and H.Y. performed the Rab9 study. T.M. developed the Lamp2 immunofluorescence assay. M.K. provided the *Atg7*$^{-/-}$ cells. K.O. contributed data analysis. Y.T. supervised data interpretation. S.S. designed the research and wrote the paper.

Author Information Reprints and permissions information is available at www.nature.com/reprints. Correspondence and requests for materials should be addressed to S.S. (shimizu.pcb@mri.tmd.ac.jp).

METHODS

Antibodies and chemicals. Anti-Ulk1 (A7481) polyclonal antibodies were purchased from Sigma-Aldrich, and anti-Gapdh (6G7) monoclonal antibodies were purchased from BD Biosciences. Anti-LC3 (5F10) monoclonal antibodies were obtained from NanoTools, and anti-Lamp2 (GL2A7) monoclonal antibodies were obtained from Abcam. Lysosome protease inhibitor cocktail (containing 1.5 mM E-64, 2 mM leupeptin and 1 mM pepstatin A) was purchased from Nacalai Tesque. Etoposide and bafilomycin A1 were from Sigma-Aldrich, and other chemicals were purchased from Nacalai Tesque.

Cell culture and DNA transfection. MEFs generated from WT and *Atg5*$^{-/-}$ embryos at embryonic day 13.5 were immortalized with SV40 T antigen. MEFs were grown in modified DMEM[27]. Cells (10^6) were transfected with plasmid DNA using the Amaxa electroporation system (kit V, program U-20) in accordance with the manufacturer's instructions. The transfection efficiency was more than 75%, as assessed by co-transfection with DNA for GFP. The siRNA sequences used were as follows: mouse *Ulk1*, 5′-GGGUGGACACAUGCUAAUA-3′; separate mouse *Ulk1*, 5′-GGAAACUUCAGAUGUUUAA-3′; mouse *Fip200*, 5′-CCCAAAGAUUAUUCAACCA-3′; mouse beclin 1, 5′-GGUUUGGAAAGAUGCUUUA-3′; separate mouse beclin 1, 5′-GACAGUUUGGCACAAUCAA-3′; mouse *Vps34*, 5′-GAAAGAUAGUCAAACUUCA-3′; mouse *Rab9*, 5′-GCAGUACUAUUAAAGAUUATT-3′. We also used control siRNA (Dharmacon siGENOME Non-Targeting siRNA#1 D-001210-01-20; Thermo Scientific). Cells (10^6) were transfected with 10 μg of siRNA with the use of the Amaxa electroporation system.

The retroviral GFP fusion expression vectors pMSCV–GFP–MCS–Zeo and pMSCV–MCS–GFP–Zeo were constructed by replacing the HindIII–ClaI fragment of pMSCV puro (Clontech) with the Zeocin resistance gene and subsequently cloning the enhanced GFP (EGFP) sequence into the BglII site and EcoRI site, respectively. cDNA corresponding to mouse Rab9a and its mutants, mouse syntaxin7 and mouse M6PR, was subsequently cloned into these vectors to generate pMSCV–GFP–Rab9a–Zeo, pMSCV–GFP–Syntaxin7–Zeo, pMSCV–M6PR–GFP–Zeo, pMSCV–GFP–Rab9a^{S21N}–Zeo and pMSCV–GFP–Rab9a^{Q66L}–Zeo. Each EGFP fusion plasmid was introduced into the MEFs by retroviral infection with the use of Plat-E cells.

Quantitative RT–PCR and microarray analysis. *Atg5*$^{-/-}$ MEFs were incubated with or without 10 μM etoposide for 12 h, and microarray analysis and qRT–PCR were performed. For microarray analysis, total RNA was purified with TRIzol reagent (Invitrogen) and used for preparing cRNA by Message AmpII (Ambion). cRNA was hybridized to Mouse Whole Genome 4 × 44K microarrays (Agilent Technologies) in accordance with the manufacturer's instructions. Two biological replicates were performed for each set of experimental conditions. Data were analysed with Feature Extraction Software (v. 9.5.3.1) (Agilent). For qRT–PCR analysis, total RNA was purified on an RNeasy column (Qiagen) and used for mRNA purification by Turbo Capture8 (Qiagen). Synthesis of cDNA and PCR amplification were performed with the iScript One-step RT–PCR kit with SYBR Green (Bio-Rad). Quantitative determination was performed with the CFX96 real-time PCR system (Bio-Rad). All samples were normalized for *Gapdh* level.

Electron microscopy. Attached cells and tissues were fixed by a conventional method (1.5% paraformaldehyde and 3% glutaraldehyde in 0.1 M phosphate buffer, pH 7.3, followed by an aqueous solution of 1% OsO_4) or by a quick-freeze substitution method (cells were frozen in liquid nitrogen and then fixed with 1% OsO_4 in acetone at −80 °C). Fixed samples were embedded in Epon 812, and thin sections (70–80 nm) were then cut and stained with uranyl acetate and lead citrate for observation under a Jeol-1010 electron microscope (Jeol) at 80 kV.

Fixed adherent cells were sectioned up to 3 μm from the base. The extent of macroautophagy was assessed on electron micrographs that contained both the nucleus and cytoplasm of individual cells. The area of every autophagic vacuole and total cytoplasmic area were calculated on the enlarged photographs with the use of a planimeter (Planix). For each cell, the autophagic area was calculated by expressing the total area of autophagic vacuoles as a percentage of the cytoplasmic area, and cells with an autophagic area of more than 6% were defined as autophagic cells (6% was the upper limit in healthy cells). Macroautophagy was quantified in each sample for at least 20 cells and was confirmed by two additional independent experiments.

In experiments combining fluorescence microscopy and electron microscopy, MEFs cultured on coverslips with grids were treated with 10 μM etoposide for 18 h and fixed with glutaraldehyde and paraformaldehyde. In the Lamp2 experiment, cells were immunostained with anti-Lamp2 monoclonal antibody. Subsequently, three or four sections were acquired under confocal fluorescence microscopy and the cells were treated with OsO_4. Cells were identified by using the grid as a guide, and the same sections as those employed for fluorescence analysis were also examined by electron microscopy. In the GFP–LC3 experiment, after GFP–LC3 fluorescence had been viewed, the same cells were fixed with OsO_4 and examined by electron microscopy.

The number of autophagic vacuoles and mitochondria in erythrocytes or reticulocytes was counted in cells that had a long axis of more than 4.5 μm.

Long-lived protein degradation assay. MEFs were starved or treated with etoposide with zVAD-fmk (100 μM), and degradation of long-lived proteins was measured by a standard method[28]. In brief, cells were labelled for 20 h with a medium containing 0.2 μCi ml^{-1} L-[^{14}C]valine (GE Healthcare). After washing and incubation in a medium containing 10 mM unlabelled valine for 60 min, the medium was replaced with fresh medium and the incubation was continued for the indicated durations. The medium was then precipitated in 10% trichloroacetic acid (TCA), and TCA-soluble radioactivity was measured. Release of [^{14}C]valine was calculated from the radioactivity in the TCA-soluble supernatant as a percentage of the total cell radioactivity. The extent of protein degradation was calculated by subtracting [^{14}C]valine release by untreated cells from that by starved or etoposide-treated cells, as the percentage of protein degradation in stress-induced cells minus the percentage of protein degradation in healthy cells.

Staining of conventional macroautophagosomes. Cells stably expressing GFP–LC3 were treated with etoposide or subjected to starvation, and the fluorescence of attached cells was observed under an FV500 confocal fluorescence microscope (Olympus) after 18 h.

Immunofluorescence analysis. Cells grown in eight-well slide chambers were fixed in 4% formaldehyde, permeabilized in 0.1% Triton X-100 and stained with anti-Lamp2 monoclonal antibody, followed by a FITC-conjugated secondary antibody (Invitrogen). The coverslips were then mounted in mounting medium (Beckman Coulter) with propidium iodide and examined by fluorescence microscopy.

Statistical analysis. Statistical evaluation was performed with the non-paired *t*-test.